# Expansion of Human iPSC-Derived Ureteric Bud Organoids with Repeated Branching Potential

AUTHOR(S):

Mae, Shin-Ichi; Ryosaka, Makoto; Sakamoto, Satoko; Matsuse, Kyoko; Nozaki, Aya; Igami, Maiko; Kabai, Ryotaro; Watanabe, Akira; Osafune, Kenji

CITATION:

Mae, Shin-Ichi ...[et al]. Expansion of Human iPSC-Derived Ureteric Bud Organoids with Repeated Branching Potential. Cell Reports 2020, 32(4): 107963.

ISSUE DATE:

2020-07-28

URL:

http://hdl.handle.net/2433/253549

Report

Cell Reports

# Expansion of Human iPSC-Derived Ureteric Bud Organoids with Repeated Branching Potential

## Graphical Abstract

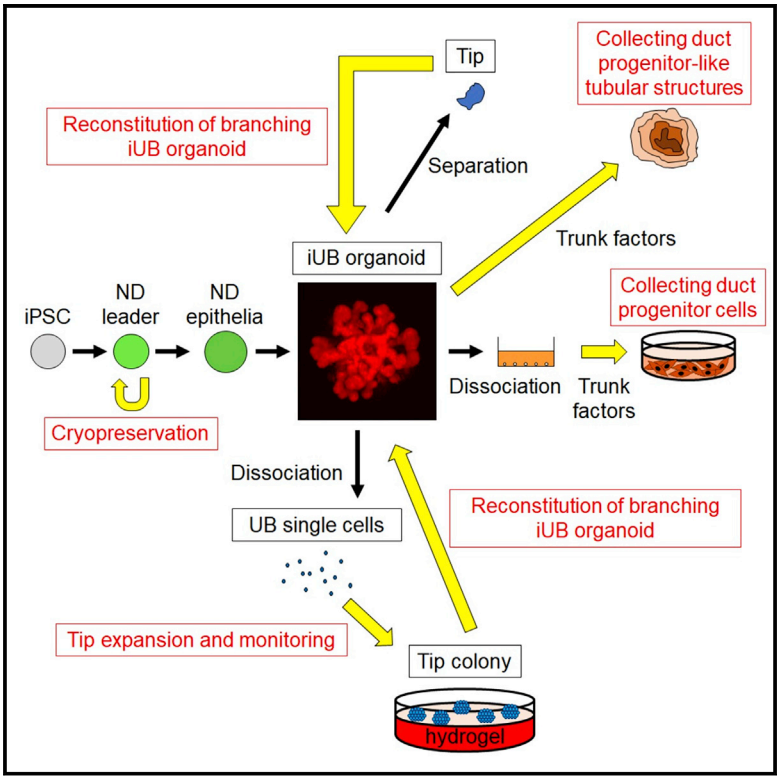


## Highlights

- Induced ureteric bud (iUB) organoids have tubular lumens and repeat branching
- *In vitro* monitoring and expansion methods for UB tip cells are established
- iUB organoids can be differentiated into collecting duct progenitors
- iUB organoids can be used to model multicystic dysplastic kidney (MCDK)

## Authors

Shin-Ichi Mae, Makoto Ryosaka, Satoko Sakamoto, ..., Ryotaro Kabai, Akira Watanabe, Kenji Osafune

## Correspondence

osafu@cira.kyoto-u.ac.jp

## In Brief

Mae et al. generate induced ureteric bud (iUB) organoids from hiPSCs that have tubular lumens and repeat branching. They also establish *in vitro* monitoring and expansion methods for UB tip cells that reconstitute iUB organoids and differentiate into collecting duct progenitors. iUB organoids can be used to model MCDK.

Mae et al., 2020, Cell Reports *32*, 107963
July 28, 2020 
https://doi.org/10.1016/j.celrep.2020.107963

CellPress

Cell Reports

CellPress OPEN ACCESS

Report

# Expansion of Human iPSC-Derived Ureteric Bud Organoids with Repeated Branching Potential

Shin-Ichi Mae,[1,3] Makoto Ryosaka,[1,3] Satoko Sakamoto,[2] Kyoko Matsuse,[1] Aya Nozaki,[1] Maiko Igami,[1] Ryotaro Kabai,[2] Akira Watanabe,[2] and Kenji Osafune[1,4,*]

[1]Center for iPS Cell Research and Application (CiRA), Kyoto University, 53 Kawahara-cho, Shogoin, Sakyo-ku, Kyoto 606-8507, Japan
[2]Medical Innovation Center, Graduate School of Medicine, Kyoto University, 53 Kawahara-cho, Shogoin, Sakyo-ku, Kyoto 606-8507, Japan
[3]These authors contributed equally
[4]Lead Contact
*Correspondence: osafu@cira.kyoto-u.ac.jp
https://doi.org/10.1016/j.celrep.2020.107963

## SUMMARY

Ureteric bud (UB) is the embryonic kidney progenitor tissue that gives rise to the collecting duct and lower urinary tract. UB-like structures generated from human pluripotent stem cells by previously reported methods show limited developmental ability and limited branching. Here we report a method to generate UB organoids that possess epithelial polarity and tubular lumen and repeat branching morphogenesis. We also succeed in monitoring UB tip cells by utilizing the ability of tip cells to uptake very-low-density lipoprotein, cryopreserving UB progenitor cells, and expanding UB tip cells that can reconstitute the organoids and differentiate into collecting duct progenitors. Moreover, we successfully reproduce some phenotypes of multicystic dysplastic kidney (MCDK) using the UB organoids. These methods will help elucidate the developmental mechanisms of UB branching and develop a selective differentiation method for collecting duct cells, contributing to the creation of disease models for congenital renal abnormalities.

## INTRODUCTION

The mammalian adult kidney, metanephros, develops by the reciprocal interaction between two embryonic progenitor tissues, metanephric mesenchyme and ureteric bud (UB) (Costantini and Kopan, 2010). UB has epithelial polarity and tubular lumen (Meyer et al., 2004) and consists of two domains, the tip and trunk. The tip cells produce both new tip and trunk cells that further differentiate into collecting ducts (CDs). Nephron progenitors (NPs) included in metanephric mesenchyme secrete glial cell-derived neurotrophic factor (GDNF) to maintain the proliferation and regulate the branching morphogenesis of UB cells and also undergo a mesenchymal-to-epithelial transition to form nephron structures (Costantini and Kopan, 2010; Takahashi, 2001).

Congenital anomalies of the kidney and urinary tract (CAKUT) describe a group of disorders that result from the developmental abnormalities of CD lineage cells, such as multicystic dysplastic kidney (MCDK) (Yosypiv, 2012). In addition to conventional experimental animal models, the creation of *in vitro* disease models using human cells for CAKUT can provide powerful research tools for pathological analyses and the development of novel therapies. Indeed, a recent study generated patient-specific human induced pluripotent stem cells (hiPSCs) from small volumes of urine from pediatric CAKUT patients and differentiated them into kidney organoids, showing the use of urine as a reliable source of hiPSCs from CAKUT patients (Mulder et al., 2020). In order to extend the findings and generate disease models for many CAKUT forms, the establishment of selective differentiation and expansion culture methods for CD lineage cells derived from hiPSCs and human embryonic stem cells (hESCs) is required.

Recently, we reported a stepwise protocol to induce hiPSCs/ESCs into UB-like structures through anterior intermediate mesoderm (Mae et al., 2013, 2018). However, the generation of hiPSC/ESC-derived UB-like tissues that show tubular lumens or sufficient branching have not been achieved (Mae et al., 2018; Taguchi and Nishinakamura, 2017; Xia et al., 2013).

In the present study, we established a method to induce hiPSCs to differentiate into UB organoids with epithelial polarity and tubular lumens that repeat branching morphogenesis. The isolated tip regions from the UB organoids showed repeated branching to reconstitute the UB organoids. We also succeeded in establishing *in vitro* monitoring and expansion methods for tip cells that could efficiently reconstitute UB organoids and differentiate into CD progenitors (CDPs). Finally, we developed a disease model for MCDK using the UB organoids.

## RESULTS

### Generation of UB Organoids that Have Tubular Lumens and Show Repeated Branching Morphogenesis

We first modified our previously reported nephric duct (ND) induction method by adding a retinoic acid (RA) agonist, 4-[(E)-2-(5,6,7,8-tetrahydro-5,5,8,8-tetramethyl-2-naphthalenyl)-1-propenyl]-benzoic acid (TTNPB), to stage 4, because RA signals

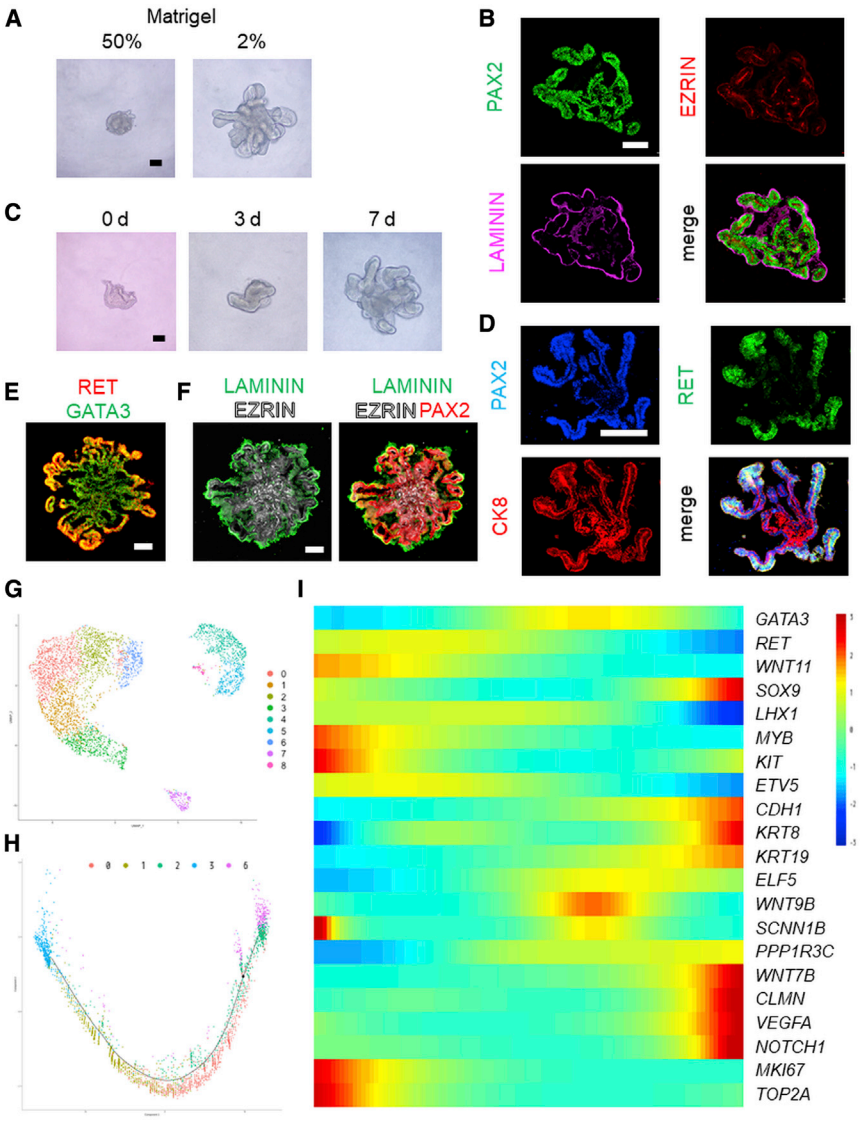


**Figure 1. iUB Organoids Have Tubular Lumens and Show Repeated Branching Morphogenesis**

(A) Morphology of stage 6 day 7 aggregates cultured with high (50%, left panel) and low (2%, right panel) concentrations of Matrigel.

(B) Immunostaining of a day 6 iUB organoid for PAX2 (green), EZRIN (red), and LAMININ (purple).

(C) Morphological changes of a tip separated from a day 6 iUB organoid for 7 days.

(D) Immunostaining of a day 14 tip-derived organoid for PAX2 (blue), RET (green), and CK8 (red).

(E and F) Immunostaining of a day 6 iUB organoid cultured in organoid medium for RET (red) and GATA3 (green) (E), and for LAMININ (green), EZRIN (white), and PAX2 (red) (F).

(G) A UMAP plot exhibiting nine clusters in iUB organoid.

(H) Pseudo-time trajectory using Monocle2.

(I) A heatmap showing the expression pattern of UB markers, HIF1α downstream genes, *VEGFA* and *NOTCH1*, and cell proliferative markers, *MKI67* and *TOP2A*, along the pseudo-time axis.

All data were obtained from cryopreserved UB progenitors. Scale bars, 100 μm.

play crucial roles in ND development (Stewart and Bouchard, 2014) (Table S1). We also found that prolonged treatment with the ND elongation factors used at stage 4 induced the epithelialization of ND cells (data not shown). Therefore, we generated ND epithelial aggregates at stage 5 by using the same inducing factors as stage 4 and removed unwanted cells by pipetting (Figure S1A). Importantly, we found that ND leading edge cells at stage 4 can be stocked with a commercially available cryopreservation reagent. The stocked cells maintain the potential to form ND epithelial aggregates to the same extent as non-cryopreserved ND leading edge cells (Figures S1B and S1C). We thus used these cryopreserved cells in most of the following examinations. The addition of low concentrations of Matrigel to the culture media was reported to promote the formation of apicobasal polarity in inner ear organoids (Koehler et al., 2017). Accordingly, we added a low concentration (2%) of Matrigel to our ND aggregates at stage 6, which effectively induced UB (iUB)-like structures (Figures 1A and S1D). Unlike our previous UB-like structures, immunostaining showed that the current ones expressed not only a basal marker, LAMININ, but also an apical marker, EZRIN, indicating that these structures have apicobasal polarity and tubular lumens, in addition to the formation of $RET^+$ tip and $CK8^+$ trunk domains (Figures 1B and S1E–S1H). The presence of tubular lumens was also shown by toluidine blue staining of the current UB-like structures (Figure S1I). Thus, we induced UB structures with tip/trunk domains, epithelial polarity, and tubular lumens, and hereafter call these structures iUB organoids. We then manually separated the tips from the iUB organoids and cultured them in stage 6 medium (Figures S2A and S2B). The separated tips formed branching structures with tip and trunk regions and epithelial polarity similar to the original iUB organoids, suggesting the reconstitution of iUB organoids (Figures 1C, 1D, and S2C). Moreover, the tips separated from the reconstituted iUB organoids also reconstituted iUB organoids with branching morphogenesis. This reconstitution process could be repeated 3–4 times for each tip, and each tip could branch 4–5 times, meaning one tip could branch maximally 20 times (Figure S2D). Furthermore, we found that adding epidermal growth factor (EGF) and fibroblast growth factor 1 (FGF1) to stage 6 medium (hereafter called organoid medium) promoted budding with tip and trunk structures and epithelial polarity (Figures 1E, 1F, and S2E–S2G; Table S1).

Next, we performed single-cell RNA sequencing (scRNA-seq) to dissect cell types in the iUB organoid and conducted

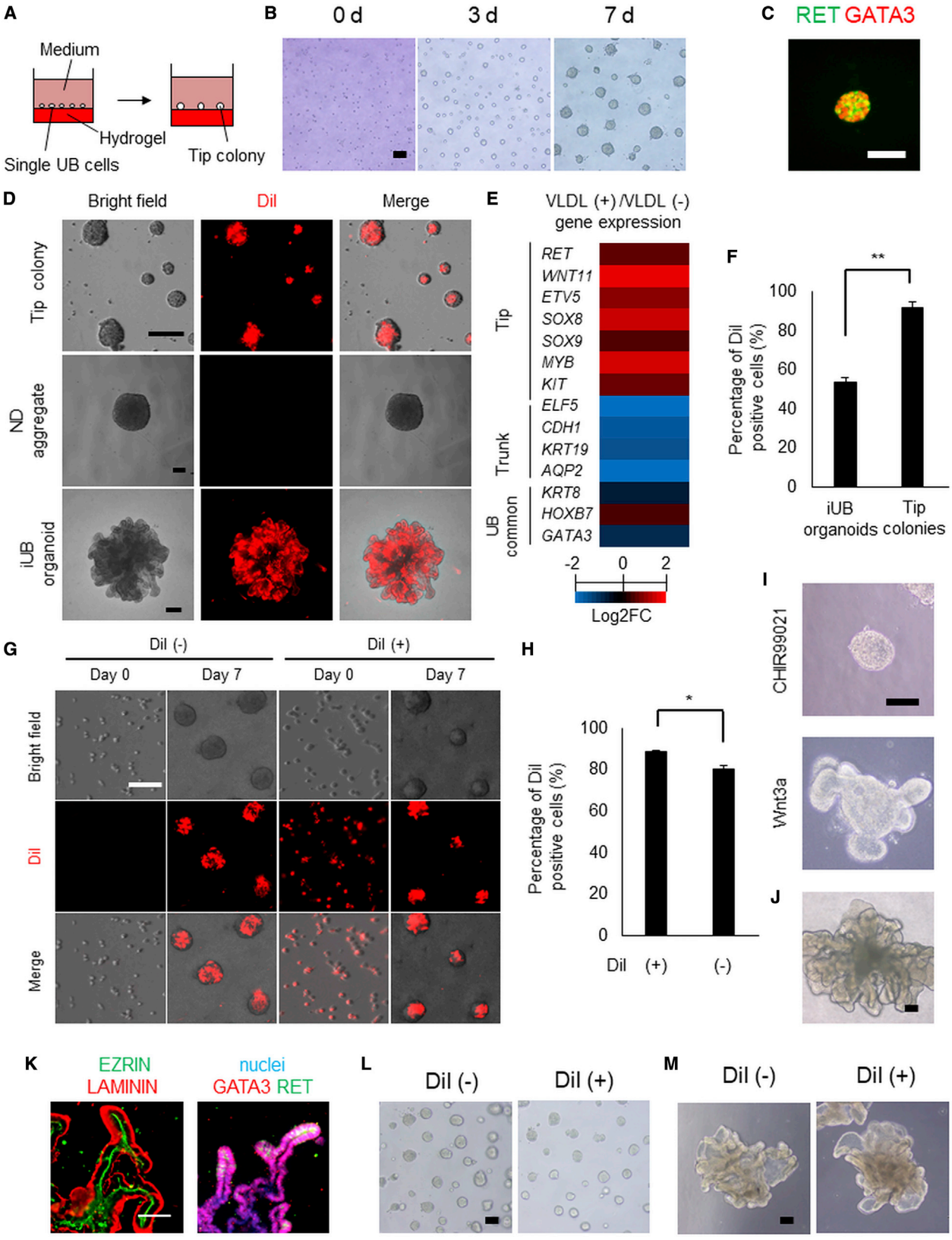


*(legend on next page)*

dimensionality reduction to cluster cells with similar gene expression profiles using Uniform Manifold Approximation and Projection (UMAP). We found that *GATA3*-expressing cell aggregate (clusters 0, 1, 2, 3, and 6) (Figures 1G and S3A) exhibited a heterogenous expression of *RET*, *WNT11*, *ETV5*, and *KRT19* among clusters (Figures S3B and S3C). Thus, we assumed that cells in clusters 0, 2, and 6 with *RET* expression were located on the tips of iUB organoid, while the trunk consisted of cells in clusters 1 and 3 with *KRT19* expression. Additionally, we found that iUB organoid contained off-target cells that resemble *MEIS2*-expressing peri-UB mesenchyme-like cells (clusters 4 and 5) and *SOX2*-expressing neural cells (cluster 8) (Figure S3D). Comparative expression analysis showed that hypoxia inducible factor 1α (HIF-1α)-induced genes, including *VEGFA* and *NOTCH1*, were upregulated in trunk cells (Table S2), whereas tip cells highly but differentially expressed the cell proliferation markers *MKI67* and *TOP2A* (Figure S3D). We also found HOX family genes were differentially expressed between the tip and trunk clusters (Figure S3E). However, a previous study reported no segmental specificity of Hox gene expression in developing mouse UBs based on *in situ* hybridization (Patterson and Potter, 2004). Future studies should examine whether segmental regulation is involved in iUB formation. We then addressed transcriptional dynamics during iUB organoid formation by trajectory analysis using Monocle2. As with the UMAP, cells were roughly lined up in the order of clusters 6, 2, 0, 1, and 3 (Figure 1H). In the pseudo-time axis, cells on the left side were tip cells expressing *RET* and *ETV5*, whereas cells on the right side were trunk cells with high expression of *KRT8* and *KRT19*, as well as *VEGFA* and *NOTCH1* (Figure 1I). Interestingly, *RET* expression was broadly increased on the left side compared with the right side. However, the peak expression was not at the very left edge but a little before there, whereas the highest expression of *MKI67* and *TOP2A* was observed at the very left edge (Figure 1I), indicating that cells at the left edge were proliferating tip cells. These results are consistent with previous *in vivo* findings that *Ret* expression is dominant at the broad tip rather than distal tip (Rutledge et al., 2017), and that tip cells act as proliferative stem cells in the mouse UB branching process (Shakya et al., 2005). We therefore successfully generated iUB organoids with epithelial polarity and tubular lumens consisting of distinct tip and trunk cells, and show the developmental potential to repeat branching morphogenesis.

## Monitoring and Expansion Culture of Tip Cells

We next found that dissociated single iUB cells successfully expanded to form colonies on soft hydrogel that resembled tip regions expressing RET and GATA3 (Figures 2A–2C). To reveal the origin of the tip colonies, we attempted to develop methods to monitor tip cell development. Consistent with a previous report, we found that very-low-density lipoprotein (VLDL) receptor is expressed at the tip regions by immunostaining analysis (Rutledge et al., 2017) (Figure S4A). We also confirmed that whole tip colonies and tip regions of iUB organoids, but not ND aggregates, imported VLDL conjugated with 1,1'-Dioctadecyl-3,3,3',3'-Tetramethylindocarbocyanine Perchlorate (DiI) (DiI-VLDL) (Figure 2D). Additionally, RNA-seq comparing $DiI^+$ and $DiI^-$ cells purified by flow cytometry indicated the upregulated expression of tip-related genes in $DiI^+$ cells, but the expression of trunk-related genes was higher in $DiI^-$ cells (Figure 2E). This monitoring technique clarified that the percentage of $DiI^+$ tip cells increased from 54.0% ± 2.1% to 91.8% ± 2.8% after 7 days by our hydrogel culture (n = 3; Figure 2F). Interestingly, tip colonies importing DiI-VLDL were derived from not only $DiI^+$ cells, but also $DiI^-$ cells after 7 days (Figure 2G). The percentage of tip cells derived from $DiI^-$ cells was high at 80.5% ± 1.6%, although significantly lower than that derived from $DiI^+$ cells (88.9% ± 0.5%; Figure 2H). These results are consistent with the previous finding that UB trunk cells can regenerate tip cells *in vitro* (Yuri et al., 2017).

In order to establish a robust reconstitution method of iUB organoids from tip colonies, we focused on the Wnt signaling pathway and replaced CHIR99021 with Wnt3a conditioned medium and R-spondin1 in organoid medium (hereafter called modified medium). Consequently, we found that branching iUB organoids with tip and trunk regions and epithelial polarity could be reconstituted from tip colonies with modified medium (Figures 2I–2K). Importantly, iUB organoids could be reconstituted from not only $DiI^+$ tip single cells, but also $DiI^-$ trunk single cells (Figures 2L and 2M). Moreover, we found that tip regions separated from iUB organoids derived from single iUB cells via tip colonies reconstituted iUB organoids, demonstrating the establishment of a simplified expansion method of tip cells with the developmental potential to form iUB organoids (Figure S4B). To elucidate the developmental mechanism of iUB organoid reconstitution from tip colonies, we added a Notch

**Figure 2. Monitoring and Expansion Methods for Tip Cells**

(A) A schematic showing the formation of tip colonies from single iUB cells on hydrogel.
(B) Morphological changes of single iUB cells dissociated from iUB organoids for 7 days.
(C) Immunostaining of a day 7 tip colony for RET (green) and GATA3 (red).
(D) Bright-field and fluorescence microscopy images of tip colonies, a ND aggregate, and an iUB organoid after DiI-VLDL uptake.
(E) A heatmap showing differentially expressed genes between $DiI^+$ and $DiI^-$ cells evaluated by RNA-seq.
(F) The percentage of $DiI^+$ cells in day 7 iUB organoids and day 7 tip colonies.
(G) Fluorescence microscopy analysis of $DiI^-$ and $DiI^+$ cells on days 0 and 7.
(H) The percentage of $DiI^+$ cells in day 6 tip colonies derived from single $DiI^+$ and $DiI^-$ cells.
(I) Morphology of day 7 iUB organoids reconstituted from tip colonies in organoid medium containing CHIR99021 or Wnt3a.
(J) Morphology of a day 18 iUB organoid reconstituted from a tip colony in modified medium.
(K) Immunostaining of a day 18 reconstituted iUB organoid for EZRIN (green) and LAMININ (red) (left panel) and for RET (green), GATA3 (red), and nuclei (blue) (right panel).
(L) Morphology of day 7 tip colonies derived from $DiI^-$ (left panel) and $DiI^+$ (right panel) single iUB cells.
(M) Morphology of day 16 iUB organoids reconstituted from tip colonies derived from $DiI^-$ (left panel) and $DiI^+$ (right panel) single iUB cells.
All data were obtained from cryopreserved UB progenitors. *$p < 0.05$, **$p < 0.001$, by Student's t test in (F) and (H). Scale bars, 100 μm.

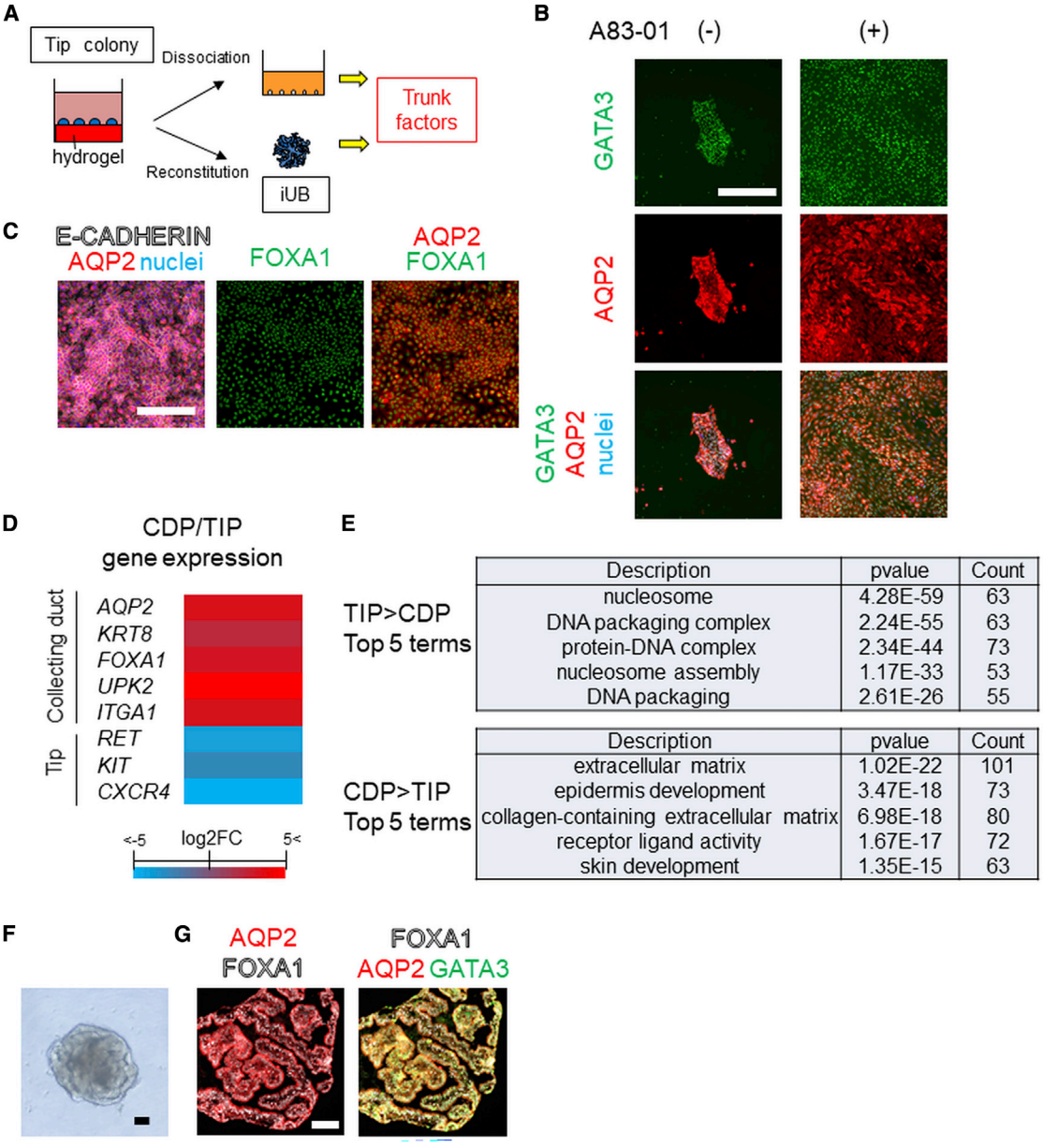


| Description | pvalue | Count |
|---|---|---|
| nucleosome | 4.28E-59 | 63 |
| DNA packaging complex | 2.24E-55 | 63 |
| protein-DNA complex | 2.34E-44 | 73 |
| nucleosome assembly | 1.17E-33 | 53 |
| DNA packaging | 2.61E-26 | 55 |

| Description | pvalue | Count |
|---|---|---|
| extracellular matrix | 1.02E-22 | 101 |
| epidermis development | 3.47E-18 | 73 |
| collagen-containing extracellular matrix | 6.98E-18 | 80 |
| receptor ligand activity | 1.67E-17 | 72 |
| skin development | 1.35E-15 | 63 |

**Figure 3. Induction of CDPs**

(A) A schematic showing the induction methods of CDPs.

(B) Immunostaining of dissociated tip colony cells on day 7 in 2D culture with or without A83-01 for GATA3 (green), AQP2 (red), and nuclei (blue).

(C) Immunostaining of dissociated tip colony cells on day 7 in 2D culture for AQP2 (red), E-CADHERIN (white), nuclei (blue), and FOXA1 (green).

(D) A heatmap showing differentially expressed genes between CDPs and tip colony (TIP) cells evaluated by RNA-seq.

(E) The top 5 Gene Ontology biological processes for the significantly differentially expressed ($p < 0.05$) genes between CDPs and TIP cells.

(F and G) Morphology (F) and immunostaining images of day 28 CDP-like tubular structures derived from a day 14 reconstituted iUB organoid from a tip colony for FOXA1 (white), AQP2 (red), and GATA3 (green) (G).

All data were obtained from cryopreserved UB progenitors. Scale bars, 100 μm.

signaling inhibitor, [N-[N-(3,5-Difluorophenacetyl-L-alanyl)]-S-phenylglycine tert.butyl ester] (DAPT), to modified medium according to the scRNA-seq data (Figure 1I). The resultant inhibition of budding structure formation by DAPT treatment indicated that Notch signaling is involved in iUB formation (Figure S4C).

## Induction of CDPs

Because Wnt/β-catenin signals maintain stem cells in UB tip regions (Yuri et al., 2017), we retrieved tip colonies from the hydrogel and cultured them using a WNT signal inhibitor, IWR-1 (Figure 3A). IWR-1 treatment facilitated the differentiation of dissociated tip cells into cells expressing a CD principal cell

marker, Aquaporin 2 (AQP2) (Figure 3B). We also found that combination treatment with IWR-1 and a TGFβ signal inhibitor, A83-01, more efficiently generated AQP2$^+$ cells (Figure 3B). These cells also expressed a trunk-specific marker, FOXA1, but not an intercalated cell marker, carbonic anhydrase (CA) II, suggesting the development of CDPs (Figures 3C and S4D). RNA-seq indicated that some marker genes for CD principal cells, such as *AQP2* and *FOXA1*, are expressed in CDPs; however, neither other principal cell markers, *AQP3* and *AQP4*, nor intercalated cell markers, *FOXI1* and *V-type proton ATPase subunit B, kidney isoform* (*ATP6V1B1*), were expressed (Figures 3D, S4E, and S4F). Gene Ontology (GO) analysis also showed relevant biological processes for tip colonies and CDPs (Figure 3E). Specifically, cell proliferation-related genes were upregulated in tip colonies, while extracellular matrix and receptor-related genes were expressed in CDPs. Thus, these induced CDPs may correspond to around gestational week (GW) 7 CDPs, which express only principal cell markers (Wang et al., 2018). Moreover, we found that the same two-factor treatment differentiated reconstituted iUB organoids derived from tip colonies into AQP2$^+$ CDP-like tubular structures (Figures 3F and 3G).

### Generation of an MCDK Disease Model Using HNF1β$^{+/-}$ iUB Organoids

Finally, we attempted to establish a CAKUT disease model using our current iUB organoid technique. The mutations of a UB lineage marker, *HNF1β*, are associated with renal hypoplasia and MCDK (Bellanné-Chantelot et al., 2004; Heidet et al., 2010; Nakayama et al., 2010). A mouse model with CD-specific deletion of Hnf1β showed the abnormalities of ductal apicobasal polarity (Desgrange et al., 2017; De Vas et al., 2015). We thus established a heterozygous HNF1β-knockout (HNF1β$^{+/-}$) hiPSC line by the CRISPR-Cas9 system (Figure 4A). Although this cell line could be differentiated into iUB organoids, these organoids were phenotypically different from wild-type (WT) iUB organoids in that the number of budding regions tends to be reduced (Figure 4B). Immunostaining showed that RET$^+$ tip regions in HNF1β$^{+/-}$ iUB organoids were smaller than those in WTs (Figure 4C), and that apicobasal polarity was lost in HNF1β$^{+/-}$ iUB organoids, as evidenced by the reduced expression of apical markers, PRKCζ and EZRIN (Figures 4D and S4G). Additionally, we confirmed that the expressions of *PRKCζ* and *EZRIN* (relative expressions compared with WT were 0.61 ± 0.18, p = 0.021, and 0.75 ± 0.11, p = 0.016, respectively), and UB lineage markers downstream of *HNF1β*, *LHX1*, and *PAX2* (relative expressions compared with WT were 0.32 ± 0.28, p = 0.014, and 0.44 ± 0.21, p = 0.010, respectively), were significantly decreased in HNF1β$^{+/-}$ iUB organoids (Figure 4E). The expressions of other *HNF1β* downstream markers, *RET* and *WNT11*, tended to decrease in HNF1β$^{+/-}$ iUB organoids compared with WT, although the difference was not statistically significant (relative expressions compared with WT were 0.62 ± 0.35, p = 0.138, and 0.49 ± 0.36, p = 0.07, respectively) (Figure S4H). These findings are similar to those found in a MCDK model mouse (Lokmane et al., 2010; Desgrange et al., 2017), indicating that our iUB organoids can be used to develop disease models for one form of CAKUT.

## DISCUSSION

Previously generated UB lineage cells from hiPSCs/ESCs have limitations. Takasato et al. (2015) reported that the GATA3$^+$ECADHERIN$^+$ cells contained in their kidney organoids are UB lineage. However, their organoids lacked branching UB structures, and scRNA-seq of the organoids indicated that these cells could be distal tubules or connecting segments, which also express GATA3 and E-CADHERIN, derived from NPs (Combes et al., 2019; Lindström et al., 2018b). Additionally, although Taguchi and Nishinakamura, 2017 induced UB-like structures from hiPSCs that express SOX9 and CK8 based on quantitative real-time PCR (qRT-PCR) and immunostaining analyses, these markers are not specific to UB lineages. Thus, the generation of UB tissues with distinct tip and trunk regions from hiPSCs/ESCs has not been fully demonstrated. Importantly, we have demonstrated in the current study that our iUB organoids recapitulate *in vivo* development accompanied by spatiotemporal regulation of the gene network by high-resolution transcriptome analysis using scRNA-seq, which showed the reciprocal expression of UB tip and trunk markers.

Although the hypoxic activation of HIF increases paracrine vascular endothelial growth factor A (VEGFA) signaling to enhance UB branching (Schley et al., 2015), the developmental significance and role of the signaling in the UB trunk are unclear. During kidney development, the blood vessels first arise to form a vascular ring around the UB trunk (Munro et al., 2017). It was also reported that the branching pancreatic bud recruits blood vessels via VEGFA to enhance trunk cell maintenance and inhibit acinar cell differentiation (Cleaver and Dor, 2012). These findings, including ours, suggest that VEGFA secretion from the UB trunk may support vascular network formation in kidney development. Further studies are needed to reveal the precise interaction between hypoxia-responsive molecules and renal vascular formation.

It takes about 2 weeks to generate our iUB organoids from hiPSCs. This time might reflect an *in vivo* developmental clock, because hiPSCs are equivalent to embryonic days 6–14 (Nakamura et al., 2016) and metanephric kidney development begins at GW4 in humans (Lindström et al., 2018). In addition, a recent study reported that human CDPs expressing AQP2, but not CAII, appear at GW7 (Wang et al., 2018). This time course also coincides with our induction protocol, in which it takes about 5 weeks to differentiate AQP2$^+$CAII$^-$ progenitors from hiPSCs. Although one valuable approach to inducing AQP2$^+$ cells is a co-culture that forms aggregates from hiPSC-derived UB cells and NPs (Tsujimoto et al., 2020), the selective induction of CDPs from iUB organoid-derived expanded tip colonies established in this study without co-cultures is notably advantageous.

However, there are limitations in the current study as well. First, although we examined various co-culture conditions with iUB organoids and hiPSC-derived NPs, extensive UB branching morphogenesis was not achieved even though NPs differentiated into nephron structures (data not shown). One possible explanation is that, although interstitial cells are required for the inductive branching morphogenesis of UB by reciprocal interactions with NPs in mouse ESC differentiation culture (Taguchi and Nishinakamura, 2017), our co-culture conditions may contain no interstitial cells. Another possibility is a discrepancy in the time required for

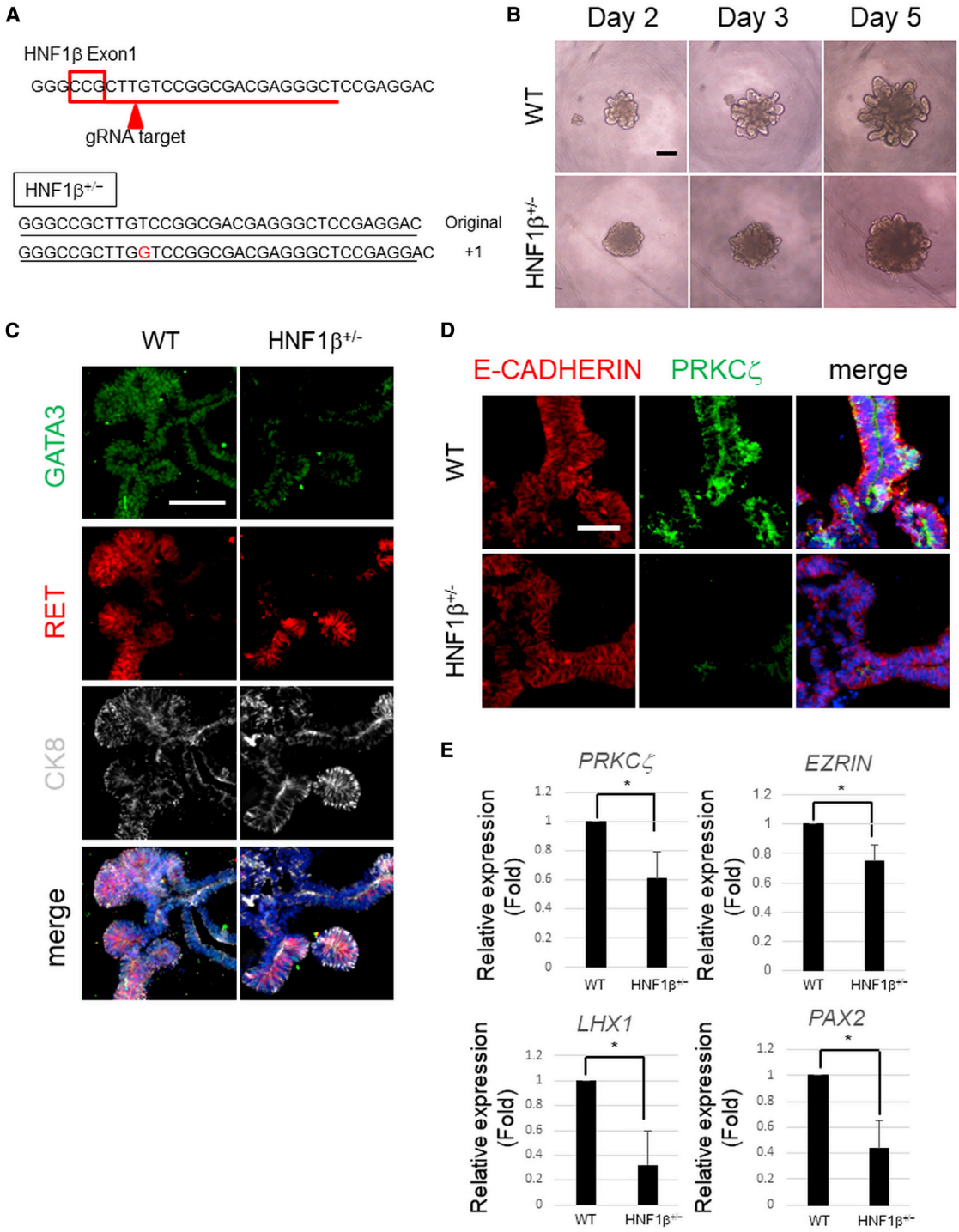


**Figure 4. Generation of an MCDK Disease Model**

(A) A part of the nucleotide sequence of HNF1β exon 1 and the guide RNA (gRNA) target region. An HNF1β$^{+/-}$ hiPSC line was established by a single-base (red) insertion.

(B) Morphological changes of ND aggregates derived from wild-type (WT) and HNF1β$^{+/-}$ hiPSCs for 5 days.

(C and D) Immunostaining of day 10 iUB organoids derived from WT and HNF1β$^{+/-}$ hiPSCs for GATA3 (green), RET (red), CK8 (white), and nuclei (blue) (C) and for E-CADHERIN (red), PRKCζ (green), and nuclei (blue) (D).

(E) qRT-PCR analysis showing the expression of *PRKCζ*, *EZRIN*, *LHX1*, and *PAX2* in WT and HNF1β$^{+/-}$ iUB organoids.

Data in (B) and (E) were obtained from cryopreserved UB progenitor cells; data in (C) and (D) were from non-cryopreserved UB progenitor cells. *$p < 0.05$ by Student's t test in (E). Scale bars, 100 μm.

the UB branching presented in this study and the mesenchymal-epithelial transition of hiPSC-derived NPs previously used (Taguchi et al., 2014; Takasato et al., 2015; Morizane et al., 2015). Future studies should examine the optimal co-culture conditions.

Second, although some phenotypes, including abnormal tubular apicobasal polarity, were successfully reproduced, cystic structures were not found in our MCDK model (data not shown). We assumed that our iUB organoids did not differentiate into mature CDs that reproduce cystic lesions. Future studies should develop induction methods, such as long-term *in vitro* culture, to generate mature CDs and model the disorders that develop CD cysts, such as MCDK, autosomal dominant polycystic kidney disease (ADPKD), and autosomal recessive polycystic kidney disease (ARPKD). These mature CD cells would also contribute to analyzing the physiological functions of human CDs, such as water and ion balance regulation after the hormonal stimulation of vasopressin and aldosterone.

In conclusion, we found that the acquisition of epithelial polarity and tubular lumens in UB-like structures leads to the development of branching iUB organoids *in vitro*. We also established a monitoring method of tip cells utilizing DiI-VLDL uptake and a simplified expansion method for tip cells that reconstitute branching iUB organoids, which differentiate into CDPs. These techniques may help elucidate the developmental mechanisms of UB branching and develop a selective differentiation method for CD cells, thereby contributing to the creation of CAKUT models caused by abnormalities arising in CDs.

## STAR★METHODS

Detailed methods are provided in the online version of this paper and include the following:

- KEY RESOURCES TABLE
- RESOURCE AVAILABILITY
  - Lead Contact
  - Materials Availability
  - Data and Code Availability
- EXPERIMENTAL MODEL AND SUBJECT DETAILS
- METHOD DETAILS
  - Anterior intermediate mesoderm induction
  - Nephric duct induction
  - iUB organoid induction
  - ND cryopreservation
  - Tip cell expansion
  - Reconstitution of iUB organoids from single tip cells
  - Collecting duct progenitor induction
  - Monitoring tip cells using DiI-VLDL
  - Flow cytometry analysis of tip cells using DiI-VLDL
  - RNA sequencing analysis
  - Single cell RNA sequencing analysis
  - Generation of heterozygous HNF1β knockout hiPSCs
  - Real-time PCR analysis
  - Immunostaining
- QUANTIFICATION AND STATISTICAL ANALYSIS
  - RNA sequencing data processing
  - Single cell RNA sequencing data processing
  - Statistical analysis

## SUPPLEMENTAL INFORMATION

Supplemental Information can be found online at https://doi.org/10.1016/j.celrep.2020.107963.

## ACKNOWLEDGMENTS

We thank Dr. Keisuke Okita, CiRA, Kyoto University, for kindly providing the cell line; Dr. Peter Karagiannis, CiRA, Kyoto University, for critically reading and revising the manuscript; and DNAFORM Co., Ltd. for technical support. This study was partially supported by Otsuka Pharmaceutical Co., Ltd., the Japan Society for the Promotion of Science (JSPS) through its Grant-in-Aid for Scientific Research (B) (JSPS KAKENHI grant 18H02826 to K.O. and grant 17K15546 to S.-I.M.), iPS Academia Japan, Inc. through its 2018 iPS Academia Japan Grant (to S.I.M.), and Japan Agency for Medical Research and Development (AMED) through its research grant "Projects for Technological Development, Core Center for iPS Cell Research and the Acceleration Program for Intractable Diseases Research Utilizing Disease-Specific iPSCs, Research Center Network for Realization of Regenerative Medicine" and "Practical Research Project for Rare/Intractable Diseases" (to K.O.).

## AUTHOR CONTRIBUTIONS

S.-I.M., M.R., A.W., and K.O. designed the study. S.-I.M., M.R., S.S., K.M., A.N., M.I., and R.K. performed the experiments. S.-I.M., M.R., S.S., R.K., A.W., and K.O. analyzed the data. K.O. supervised the study. S.-I.M., M.R., A.W., and K.O. drafted the manuscript. All authors discussed the results and commented on the manuscript.

## DECLARATION OF INTERESTS

K.O. is a founder and member without salary of the scientific advisory boards of iPS Portal, Inc., and a founder and chief scientific advisor of RegeNephro Co., Ltd.

Received: October 21, 2019
Revised: May 21, 2020
Accepted: July 3, 2020
Published: July 28, 2020

## REFERENCES

Bellanné-Chantelot, C., Chauveau, D., Gautier, J.F., Dubois-Laforgue, D., Clauin, S., Beaufils, S., Wilhelm, J.M., Boitard, C., Noël, L.H., Velho, G., and Timsit, J. (2004). Clinical spectrum associated with hepatocyte nuclear factor-1beta mutations. Ann. Intern. Med. *140*, 510–517.

Cleaver, O., and Dor, Y. (2012). Vascular instruction of pancreas development. Development *139*, 2833–2843.

Combes, A.N., Zappia, L., Er, P.X., Oshlack, A., and Little, M.H. (2019). Single-cell analysis reveals congruence between kidney organoids and human fetal kidney. Genome Med. *11*, 3.

Costantini, F., and Kopan, R. (2010). Patterning a complex organ: branching morphogenesis and nephron segmentation in kidney development. Dev. Cell *18*, 698–712.

De Vas, M.G., Kopp, J.L., Heliot, C., Sander, M., Cereghini, S., and Haumaitre, C. (2015). Hnf1b controls pancreas morphogenesis and the generation of Ngn3+ endocrine progenitors. Development *142*, 871–882.

Desgrange, A., Heliot, C., Skovorodkin, I., Akram, S.U., Heikkilä, J., Ronkainen, V.P., Miinalainen, I., Vainio, S.J., and Cereghini, S. (2017). HNF1B controls epithelial organization and cell polarity during ureteric bud branching and collecting duct morphogenesis. Development *144*, 4704–4719.

Heidet, L., Decramer, S., Pawtowski, A., Morinière, V., Bandin, F., Knebelmann, B., Lebre, A.S., Faguer, S., Guigonis, V., Antignac, C., and Salomon, R. (2010). Spectrum of HNF1B mutations in a large cohort of patients who harbor renal diseases. Clin. J. Am. Soc. Nephrol. *5*, 1079–1090.

Ishida, K., Xu, H., Sasakawa, N., Lung, M.S.Y., Kudryashev, J.A., Gee, P., and Hotta, A. (2018). Site-specific randomization of the endogenous genome by a regulatable CRISPR-Cas9 piggyBac system in human cells. Sci. Rep. *8*, 310.

Kanda, Y. (2013). Investigation of the freely available easy-to-use software 'EZR' for medical statistics. Bone Marrow Transplant. *48*, 452–458.

Koehler, K.R., Nie, J., Longworth-Mills, E., Liu, X.P., Lee, J., Holt, J.R., and Hashino, E. (2017). Generation of inner ear organoids containing functional hair cells from human pluripotent stem cells. Nat. Biotechnol. *35*, 583–589.

Lindström, N.O., Tran, T., Guo, J., Rutledge, E., Parvez, R.K., Thornton, M.E., Grubbs, B., McMahon, J.A., and McMahon, A.P. (2018b). Conserved and Divergent Molecular and Anatomic Features of Human and Mouse Nephron Patterning. J. Am. Soc. Nephrol. *29*, 825–840.

Lokmane, L., Heliot, C., Garcia-Villalba, P., Fabre, M., and Cereghini, S. (2010). vHNF1 functions in distinct regulatory circuits to control ureteric bud branching and early nephrogenesis. Development *137*, 347–357.

Mae, S.I., Shono, A., Shiota, F., Yasuno, T., Kajiwara, M., Gotoda-Nishimura, N., Arai, S., Sato-Otubo, A., Toyoda, T., Takahashi, K., et al. (2013). Monitoring and robust induction of nephrogenic intermediate mesoderm from human pluripotent stem cells. Nat. Commun. *4*, 1367.

Mae, S.I., Ryosaka, M., Toyoda, T., Matsuse, K., Oshima, Y., Tsujimoto, H., Okumura, S., Shibasaki, A., and Osafune, K. (2018). Generation of branching ureteric bud tissues from human pluripotent stem cells. Biochem. Biophys. Res. Commun. *495*, 954–961.

Meyer, T.N., Schwesinger, C., Bush, K.T., Stuart, R.O., Rose, D.W., Shah, M.M., Vaughn, D.A., Steer, D.L., and Nigam, S.K. (2004). Spatiotemporal regulation of morphogenetic molecules during in vitro branching of the isolated ureteric bud: toward a model of branching through budding in the developing kidney. Dev. Biol. *275*, 44–67.

Morizane, R., Lam, A.Q., Freedman, B.S., Kishi, S., Valerius, M.T., and Bonventre, J.V. (2015). Nephron organoids derived from human pluripotent stem cells model kidney development and injury. Nat. Biotechnol. *33*, 1193–1200.

Mulder, J., Sharmin, S., Chow, T., Rodrigues, D.C., Hildebrandt, M.R., D'Cruz, R., Rogers, I., Ellis, J., and Rosenblum, N.D. (2020). Generation of infant- and pediatric-derived urinary induced pluripotent stem cells competent to form kidney organoids. Pediatr. Res. *87*, 647–655.

Munro, D.A.D., Hohenstein, P., and Davies, J.A. (2017). Cycles of vascular plexus formation within the nephrogenic zone of the developing mouse kidney. Sci. Rep. *7*, 3273.

Nakamura, T., Okamoto, I., Sasaki, K., Yabuta, Y., Iwatani, C., Tsuchiya, H., Seita, Y., Nakamura, S., Yamamoto, T., and Saitou, M. (2016). A developmental coordinate of pluripotency among mice, monkeys and humans. Nature *537*, 57–62.

Nakayama, M., Nozu, K., Goto, Y., Kamei, K., Ito, S., Sato, H., Emi, M., Nakanishi, K., Tsuchiya, S., and Iijima, K. (2010). HNF1B alterations associated with congenital anomalies of the kidney and urinary tract. Pediatr. Nephrol. *25*, 1073–1079.

Nojima, S., Susaki, E.A., Yoshida, K., Takemoto, H., Tsujimura, N., Iijima, S., Takachi, K., Nakahara, Y., Tahara, S., Ohshima, K., et al. (2017). CUBIC pathology: three-dimensional imaging for pathological diagnosis. Sci. Rep. *7*, 9269.

Patterson, L.T., and Potter, S.S. (2004). Atlas of Hox gene expression in the developing kidney. Dev. Dyn. *229*, 771–779.

Rutledge, E.A., Benazet, J.D., and McMahon, A.P. (2017). Cellular heterogeneity in the ureteric progenitor niche and distinct profiles of branching morphogenesis in organ development. Development *144*, 3177–3188.

Schley, G., Scholz, H., Kraus, A., Hackenbeck, T., Klanke, B., Willam, C., Wiesener, M.S., Heinze, E., Burzlaff, N., Eckardt, K.U., and Buchholz, B. (2015). Hypoxia inhibits nephrogenesis through paracrine Vegfa despite the ability to enhance tubulogenesis. Kidney Int. *88*, 1283–1292.

Shakya, R., Jho, E.H., Kotka, P., Wu, Z., Kholodilov, N., Burke, R., D'Agati, V., and Costantini, F. (2005). The role of GDNF in patterning the excretory system. Dev. Biol. *283*, 70–84.

Stewart, K., and Bouchard, M. (2014). Coordinated cell behaviours in early urogenital system morphogenesis. Semin. Cell Dev. Biol. *36*, 13–20.

Susaki, E.A., Tainaka, K., Perrin, D., Yukinaga, H., Kuno, A., and Ueda, H.R. (2015). Advanced CUBIC protocols for whole-brain and whole-body clearing and imaging. Nat. Protoc. *10*, 1709–1727.

Taguchi, A., and Nishinakamura, R. (2017). Higher-Order Kidney Organogenesis from Pluripotent Stem Cells. Cell Stem Cell *21*, 730–746.e6.

Taguchi, A., Kaku, Y., Ohmori, T., Sharmin, S., Ogawa, M., Sasaki, H., and Nishinakamura, R. (2014). Redefining the in vivo origin of metanephric nephron progenitors enables generation of complex kidney structures from pluripotent stem cells. Cell Stem Cell *14*, 53–67.

Takahashi, M. (2001). The GDNF/RET signaling pathway and human diseases. Cytokine Growth Factor Rev. *12*, 361–373.

Takasato, M., Er, P.X., Chiu, H.S., Maier, B., Baillie, G.J., Ferguson, C., Parton, R.G., Wolvetang, E.J., Roost, M.S., Chuva de Sousa Lopes, S.M., and Little, M.H. (2015). Kidney organoids from human iPS cells contain multiple lineages and model human nephrogenesis. Nature *526*, 564–568.

Tsujimoto, H., Kasahara, T., Sueta, S.I., Araoka, T., Sakamoto, S., Okada, C., Mae, S.I., Nakajima, T., Okamoto, N., Taura, D., et al. (2020). A modular differentiation system maps multiple human kidney lineages from pluripotent stem cells. Cell Rep. *31*, 107476.

Wang, P., Chen, Y., Yong, J., Cui, Y., Wang, R., Wen, L., Qiao, J., and Tang, F. (2018). Dissecting the Global Dynamic Molecular Profiles of Human Fetal Kidney Development by Single-Cell RNA Sequencing. Cell Rep. *24*, 3554–3567.e3.

Xia, Y., Nivet, E., Sancho-Martinez, I., Gallegos, T., Suzuki, K., Okamura, D., Wu, M.Z., Dubova, I., Esteban, C.R., Montserrat, N., et al. (2013). Directed differentiation of human pluripotent cells to ureteric bud kidney progenitor-like cells. Nat. Cell Biol. *15*, 1507–1515.

Yosypiv, I.V. (2012). Congenital anomalies of the kidney and urinary tract: a genetic disorder? Int. J. Nephrol. *2012*, 909083.

Yu, G., Wang, L.G., Han, Y., and He, Q.Y. (2012). clusterProfiler: an R package for comparing biological themes among gene clusters. OMICS. *5*, 284–287.

Yuri, S., Nishikawa, M., Yanagawa, N., Jo, O.D., and Yanagawa, N. (2017). In Vitro Propagation and Branching Morphogenesis from Single Ureteric Bud Cells. Stem Cell Reports *8*, 401–416.

## STAR★METHODS

### KEY RESOURCES TABLE

| REAGENT or RESOURCE | SOURCE | IDENTIFIER |
|---|---|---|
| Antibodies | | |
| Mouse anti-AQP2 | Santa Cruz | Cat#sc-515770; RRID: AB_2810957 |
| Rabbit anti-CAII | Abcam | Cat#AB124687-100; RRID: AB_10972000 |
| Mouse anti-CK8 | Abcam | Cat#ab9023; RRID: AB_306948 |
| Mouse anti-E-CADHERIN | BD | Cat#610181; RRID: AB_397580 |
| Mouse anti-E-CADHERIN | R&D | Cat#AF648; RRID: AB_355504 |
| Mouse anti-EZRIN | Abcam | Cat#Ab4069; RRID: AB_304261 |
| Mouse anti-FOXA1 | Santa Cruz | Cat#sc-514695 |
| Rabbit anti-GATA3 | Cell signaling | Cat#5852S; RRID: AB_10835690 |
| Goat anti-GATA3 | R&D | Cat#AF2605; RRID: AB_2108571 |
| Rabbit anti-LAMININ | Sigma | Cat#L9393-2ML; RRID: AB_477163 |
| Rabbit anti-PAX2 | BioLegend | Cat#PRB-276P; RRID: AB_291611 |
| Goat anti-PAX2 | R&D | Cat#AF3364; RRID: AB_10889828 |
| Rabbit anti-PRKCζ | Santa Cruz | Cat#sc-216; RRID: AB_2300359 |
| Goat anti-RET | R&D | Cat#AF1485; RRID: AB_354820 |
| Mouse anti-VLDLR | Santa Cruz | Cat#sc-18824; RRID: AB_2216805 |
| Donkey anti-Mouse IgG- Alexa Fluor 488 | Thermo Fisher Scientific | Cat#A21202; RRID: AB_141607 |
| Donkey anti-Rabbit IgG- Alexa Fluor 488 | Thermo Fisher Scientific | Cat#A21206; RRID: AB_2535792 |
| Donkey anti-Goat IgG- Alexa Fluor 488 | Thermo Fisher Scientific | Cat#A11055; RRID: AB_2534102 |
| Donkey anti-Mouse IgG- Alexa Fluor 546 | Thermo Fisher Scientific | Cat#A10036; RRID: AB_2534012 |
| Donkey anti-Rabbit IgG- Alexa Fluor 546 | Thermo Fisher Scientific | Cat#A10040; RRID: AB_2534016 |
| Donkey anti-Goat IgG- Alexa Fluor 546 | Thermo Fisher Scientific | Cat#A11056; RRID: AB_2534103 |
| Donkey anti-Mouse IgG- Alexa Fluor 647 | Thermo Fisher Scientific | Cat#A31571; RRID: AB_162542 |
| Donkey anti-Rabbit IgG- Alexa Fluor 647 | Thermo Fisher Scientific | Cat#A31573; RRID: AB_2536183 |
| Donkey anti-Goat IgG- Alexa Fluor 647 | Thermo Fisher Scientific | Cat#A21447; RRID: AB_2536183 |
| Hoechst 33342 | Thermo Fisher Scientific | Cat#H1399 |
| Chemicals, Peptides, and Recombinant Proteins | | |
| A83-01 | WAKO | 035-24113 |
| Accutase | Innovative Cell Technologies | AT104 |
| Activin A | R&D | 338-AC |
| Afamin/Wnt3a CM | MBL | J-ORMW301R |
| B-27 Supplement minus vitamin A | Thermo Fisher Scientific | 12587001 |
| BMP4 | Peprotech | AF-120-05ET |
| bovine serum albumin | Nacalai tesque | 01281-84 |
| Cell recovery solution | BD | 354253 |
| CHIR99021 | Stem RD | CHIR-010 |
| DAPI | MERCK | 10236276001 |
| Dexamethasone | Wako | 047-18863 |
| DiI-conjugated VLDL | Biomedical Technologies, Inc. | BT-922 |
| DMEM/F-12, GlutaMAX | Thermo Fisher Scientific | 10565042 |
| Doxycycline | LTK Labs | D5897 |
| EDTA | Thermo Fisher Scientific | 15575020 |
| EGF | R&D | 236-EG-01M |
| Essential 6 Medium | Thermo Fisher Scientific | 1516401 |

(*Continued on next page*)

*Continued*

| REAGENT or RESOURCE | SOURCE | IDENTIFIER |
|---|---|---|
| FGF1 | R&D | 231-BC |
| FGF8 | Peprotech | 100-25 |
| GDNF | R&D | 212-GD |
| Geltrex | Thermo Fisher Scientific | A15696-01 |
| Hygromycin B | Nacalai tesque | 09287-84 |
| iMatrix-511 silk | Nippi | 892021 |
| IWR-1 | MERCK | I0161-5MG |
| LDN193189 | Axon Medchem | Axon1509 |
| Matrigel | BD | 354230 |
| normal donkey serum | MERCK | 566460 |
| Opti-MEM I Reduced Serum Media | Thermo Fisher Scientific | 31985062 |
| Puromycin | Nacalai tesque | 2945554 |
| Quadrol | Tokyo Chemical Industry | T781 |
| R-spondin 1 | R&D | 4645-RS-250 |
| Triton X-100 | Nacalai tesque | 35501-15 |
| TTNPB | Santa Cruz | sc-203303 |
| Thiazovivin | Santa Cruz | SCB-SC-361380-10 |
| Sucrose | Nacalai tesque | 30403-55 |
| STEM-CELLBANKER GMP grade | ZENOAQ RESOURCE | ZR646 |
| Stem Fit AK02N | Ajinomoto | AK02N |
| Triethanolamine | Wako | 145-05605 |
| Urea | Nacalai tesque | 35904-45 |
| Y-27632 | Wako | 034-24024 |
| Critical Commercial Assays | | |
| In-Fusion HD cloning kit | TaKaRa | 639648 |
| Lipofectamine 3000 | Thermo Fisher Scientific | L3000001 |
| NEBNext Poly(A) mRNA Magnetic Isolation Module | New England Biolabs | E7490 |
| NucleoSpin RNA XS | TaKaRa | 740902.5 |
| ReverTra Ace | TOYOBO | TRT-101 |
| RNeasy Mini Kit | QIAGEN | 74106 |
| SMART-Seq® Stranded Kit | TaKaRa | 634442 |
| SYBR Premix Ex TaqII | TaKaRa | RR-820B |
| Deposited Data | | |
| Single cell RNA sequencing analysis | This paper | GSE152685 |
| RNA sequencing data of DiI-VLDL(+)/(-) | This paper | GSE152471 |
| RNA sequencing data of TIP and CDP | This paper | GSE152470 |
| Experimental Models: Cell Lines | | |
| Human: 585A1 iPSC line | ICSCB | SKIP000858 |
| Human: 1231A3 iPSC line | ICSCB | HPS0381 |
| Human: 1383D2 iPSC line | ICSCB | HPS1005 |
| Experimental Models: Vectors | | |
| pHL-EF1α-hcPBase-A | Ishida et al., 2018 | N/A |
| pPV-H1-gRNA-mEF1α-RiH | Ishida et al., 2018 | N/A |
| pPV-TetO-SphcCas9-iC-A-EF1α-rtTA-iP | Ishida et al., 2018 | N/A |
| Oligonucleotides | | |
| Primers for Figures 4 and S4, see Table S3 | This paper | N/A |

(*Continued on next page*)

*Continued*

| REAGENT or RESOURCE | SOURCE | IDENTIFIER |
|---|---|---|
| Software and Algorithms | | |
| EZR | Kanda. 2013 | http://www.jichi.ac.jp/saitama-sct/SaitamaHP.files/statmedEN.html |
| BZ-X Analyzer | KEYENCE | BZX700 |
| R | The R Foudation | R version 3.6.1 |
| ZEN 2 blue edition | ZEISS | ZEN 2.3 (blue edition) |

## RESOURCE AVAILABILITY

### Lead Contact

Further information and requests for resources and reagents should be directed to and will be fulfilled by the Lead Contact, Kenji Osafune (osafu@cira.kyoto-u.ac.jp).

### Materials Availability

This study did not generate new unique reagents.

### Data and Code Availability

The NCBI GEO accession number for RNA sequencing data reported in this paper is GSE 152470, GSE 152471 and GSE 152685.

## EXPERIMENTAL MODEL AND SUBJECT DETAILS

Experiments using human induced pluripotent stem cells (hiPSCs) were approved by the Ethics Committee of the Department of Medicine and Graduate School of Medicine, Kyoto University. Three hiPSC lines, 585A1, 1231A3 and 1383D2, were maintained with feeder-free cultures using Stem Fit AK02N medium (Ajinomoto) on cell culture plates coated with 0.125 μg/cm$^2$ iMatrix-511 silk (Nippi). The cells were passaged using 0.5 mM EDTA/PBS (Thermo Fisher Scientific) every four days and routinely monitored for mycoplasma contamination.

## METHOD DETAILS

### Anterior intermediate mesoderm induction

hiPSCs were directed into UB lineages as described previously with some modifications (Mae et al., 2018). In detail, hiPSCs were plated at a density of 2.5 × 10$^4$ cells/cm$^2$ in 4-well culture plates (Thermo Fisher Scientific) in Stem Fit AK02N medium with 10 μM Y-27632 (WAKO) and 0.125 μg/cm$^2$ iMatrix-511 silk. After 24 h, the cells were washed with PBS and treated with Essential 6 medium (Thermo Fisher Scientific) containing 100 ng/mL Activin A (R&D Systems) and 3 μM CHIR99021 (Stem RD). After 16 - 24 h, the cells were washed with PBS and treated with Essential 6 medium containing 0.1 μM LDN193189 (Axon Medchem), 1 μM A83-01 (WAKO), 0.1 μM 4-[(E)-2-(5,6,7,8-Tetrahydro-5,5,8,8-tetramethyl-2-naphthalenyl)-1-propenyl]-benzoic acid (TTNPB; Santa Cruz Biotechnology) and 200 ng/mL fibroblast growth factor (FGF) 8 (Peprotech) for 2 days. Then the cells were replated at a density of 1 × 10$^5$ cells/cm$^2$ in Matrigel- or Geltrex (Thermo Fisher Scientific)-coated 24-well culture plates in Essential 6 medium containing the same 4 factors and 10 μM Y-27632 and incubated for an additional 24 h to induce anterior intermediate mesoderm (AIM).

### Nephric duct induction

AIM cells were treated with Essential 6 medium containing 1 μM CHIR99021, 0.1 μM LDN193189, 200 ng/mL FGF8, 100 ng/mL glial cell line-derived neurotrophic factor (GDNF; R&D Systems) and 0.1 μM TTNPB for 2 days to induce nephric duct (ND) leader cells. To enhance epithelialization in 2D cultures, AIM cells were treated with the same medium and inducing factors for 8 days. ND leader cells were dissociated into single cells by pipetting after treatment with Accutase (Innovative Cell Technologies) for 3 min at 37°C, seeded onto low-attachment 96-well plates (Sumitomo Bakelite) at a density of 1 × 10$^4$ cells/well, and treated with the same medium and factors plus 10 μM Y-27632 to induce epithelialized ND aggregates for 2 days.

### iUB organoid induction

Unwanted cells were separated from ND aggregates by pipetting (Mae et al., 2018). The ND aggregates were treated with Essential 6 medium containing 1 μM CHIR99021, 0.1 μM LDN193189, 200 ng/mL FGF8, 100 ng/mL GDNF, 0.1 μM TTNPB and 2% Matrigel for 6 days to constitute iUB organoids with epithelial polarity and tubular lumens. To enhance budding, 50 ng/mL EGF (R&D Systems) and 200 ng/mL FGF1 (R&D Systems) were added (hereafter called organoid medium). The tips were mechanically separated from the

iUB organoids and cultured in organoid medium for 6 to 14 days to reconstitute branching iUB organoids. The tips separated from the reconstituted iUB organoids were treated with organoid medium to repeatedly reconstitute iUB organoids.

### ND cryopreservation

Dissociated ND leader cells were resuspended with STEM-CELLBANKER GMP grade (ZENOAQ RESOURCE) at a dilution ratio less than $1 \times 10^6$ cells/mL/tube. The cell suspension was distributed to cryopreservation tubes. The tubes were frozen at −80°C for 24 h and moved to a liquid nitrogen cell storage tank for long-term cryopreservation. To initiate cultures, the cells were thawed using a water bath at 37°C. Then the cells were slowly resuspended with Essential 6 medium containing 10 μM Y-27632 and centrifuged at 200 *g* for 5 min at room temperature. After removal of the supernatant, the cells were resuspended with Essential 6 medium containing ND-induction factors with 10 μM Y-27632 and seeded onto low-attachment 96-well plates at a density of $1 \times 10^4$ cells/well.

### Tip cell expansion

iUB organoids were treated with Accutase for 5 min at 37°C and subsequently dissociated into single cells by pipetting. The cells were resuspended with DMEM/F12, GlutaMAX medium (Thermo Fisher Scientific) containing B-27 Supplement, minus vitamin A (Thermo Fisher Scientific), 100 ng/mL GDNF, 200 ng/mL FGF1, 0.1 μM TTNPB, 3 μM CHIR99021 and 10 μM Thiazovivin (Santa Cruz Biotechnology). The single cells obtained from 10 iUB organoids were seeded onto one well of 48-well plates coated with 150 μL hydrogel, which is composed of DMEM/F12 medium containing 50% Matrigel and was solidified for 1 h at 37°C before use. The single cells constructed tip colonies after 6-7 days. The medium was refreshed every 2 days.

### Reconstitution of iUB organoids from single tip cells

Hydrogel was dissolved with Cell Recovery Solution (BD Biosciences) for 1 h at 4°C to detach day 7 tip colonies. After washing with additional Cell Recovery Solution, the tip colonies were centrifuged at 500 *g* for 5 min at room temperature. Essential 6 medium containing 0.1 μM LDN193189, 100 ng/mL GDNF, 0.1 μM TTNPB, 200 ng/mL FGF8, 1 μM CHIR99021 or 10% Afamin/Wnt3a conditioned medium (MBL), 200 ng/mL R-spondin 1 (R&D systems), 50 ng/mL EGF, 200 ng/mL FGF1 and 10% Matrigel was applied to a tube containing tip colonies. After pipetting gently with a wide-mouth micropipette (BMBio) so not to break the colonies, the suspension was distributed to a low-attachment 35 mm dish (Sumitomo Bakelite) at 2 mL/dish. The medium was refreshed every 2 days. On day 7, 1 μM A83-01 was added to the medium and cultured for an additional 7 - 14 days.

### Collecting duct progenitor induction

For 2D cultures, day 7 tip colonies detached from hydrogel were dissociated into single cells by pipetting after treatment with Accutase for 3 min at 37°C. The single cells were resuspended with Essential 6 medium containing 1 μM IWR-1 (Tocris) and 0.25 $\mu g/cm^2$ iMatrix-511 silk with or without 1 μM A83-01 and seeded at a density of $4 \times 10^4$ cells/well in 96-well plates. For 3D cultures, day 14 reconstituted iUB organoids were treated with Essential 6 medium containing 1 μM IWR-1 and 1 μM A83-01 for 14 days.

### Monitoring tip cells using DiI-VLDL

iUB organoids, tip colonies and ND aggregates were treated with 10 μg/mL DiI-conjugated VLDL (Biomedical Technologies, Inc.) for 2 h at 37°C.

### Flow cytometry analysis of tip cells using DiI-VLDL

iUB organoids and tip colonies treated with DiI-VLDL were dissociated into single cells by pipetting after Accutase treatment for 5 min at 37°C. After washing with DMEM/10% FBS, the cells were re-suspended with PBS/2% FBS. Dead cells stained with 4', 6-Diamidino-2-phenylindole, dihydrochloride (DAPI; 0.1 ng/ml; Thermo Fisher Scientific) were excluded from the analysis. Single cells were analyzed and sorted using FACS Aria II (BD). Cells derived from iUB organoids and tip colonies without DiI-VLDL treatment were used as negative controls for gating.

### RNA sequencing analysis

Day 6 iUB organoids were treated with DiI-VLDL for 2 h and dissociated into single cells by pipetting after treatment with Accutase for 3 min at 37°C. Then flow cytometry analysis was performed to sort DiI-VLDL$^+$ and DiI-VLDL$^-$ cells. The total RNA of sorted DiI-VLDL$^+$ and DiI-VLDL$^-$ cells was isolated using a NucleoSpin RNA XS (TaKaRa). To analyze CDPs and TIP cells, day 10 CDPs and day 6 TIP cells were dissociated into single cells by pipetting after treatment with Accutase for 3 min at 37°C. The total RNA of each single cell was isolated using an RNeasy Mini Kit (QIAGEN). The samples were preserved at −80°C, and RNA sequence library preparation, sequencing, mapping, gene expression, and gene ontology (GO) enrichment analysis were performed by DNAFORM (Yokohama, Kanagawa, Japan).

The quality of total RNA was assessed by using a Bioanalyzer (Agilent) to ensure that RIN (RNA integrity number) was over 7.0. After poly (A) + RNA enrichment by using a NEBNext Poly (A) mRNA Magnetic Isolation Module (New England BioLabs), double-stranded cDNA libraries (RNA-seq libraries) were prepared using a SMART Seq® Stranded Kit (TaKaRa) according to the manufacturer's instructions. RNA-seq libraries were sequenced using paired end reads (50 nt of read 1 and 25 nt of read 2) on a NextSeq 500 instrument (Illumina). Obtained reads were mapped to the human GRCh38 genome using STAR (version 2.7.2b). Reads on annotated genes were counted using featureCounts (version 1.6.1).

### Single cell RNA sequencing analysis

Dissociated day 6 iUB cells were resuspended in PBS containing 1% BSA and immediately followed by library preparation targeting 5,000 cells using the Chromium Single Cell 3′ Reagent Kit v3 (10 × Genomics) and the Chromium Controller (10 × Genomics) according to manufacturer's instructions. The library was sequenced on a HiSeq2500 TruSeq SBS v3 reagent.

### Generation of heterozygous HNF1β knockout hiPSCs

We established the heterozygous HNF1β knockout hiPSC line using the CRONUS system (Ishida., et al., 2018). To generate CRONUS hiPSC lines, 1 × $10^6$ 1231A3 cells were resuspended in 100 μL of Opti-MEM (Thermo Fisher Scientific) with *piggyBac* vectors (pPV-TetO-SphcCas9-iC-A-EF1α-rtTA-iP: 2 μg, pPV-H1-gRNA-mEF1α-RiH: 2 μg) and a piggyback transpose vector (pHL-EF1α-hcP-Base-A: 2 μg). The gRNA specifically recognizing the HNF1β sequence was designed as shown in Figure 4A, and pPV-H1-gRNA-mEF1α-RiH was established using an In-Fusion HD Cloning Kit (TaKaRa). Cells were transfected with these vectors using Lipofectamine 3000 (Thermo Fisher Scientific). After lipofection, the cells were plated onto one well of a 6-well iMatrix-511 silk-coated plate in StemFit AK02N medium with 10 μM Y-27632. From the following day, the cells were treated with 1 μg/mL Puromycin (Nacalai tesque) and 200 μg/mL Hygromycin B (Nacalai tesque) for drug selection for 5 days. The expression of mRFP1 protein indicated gRNA expression. We picked up mRFP1-positive colonies and expanded them to obtain CRONUS 1231A3 cell lines. Then the cells were treated with 2 μM Dexamethasone (Wako) and 1 μM Doxycycline (LTK Labs) to induce the expression of Cas9 protein and traffic the protein to the nucleus. HNF1β mutations were confirmed using Sanger sequencing analysis. The primer sequences used are shown in Table S3.

### Real-time PCR analysis

Total RNAs isolated using the RNeasy Mini Kit (QIAGEN) were reverse-transcribed with ReverTra Ace (TOYOBO) according to the manufacturers instructions. Real-time PCR analysis was performed with SYBR Premix Ex TaqII (TaKaRa). The expression of each gene was normalized to the level of βACTIN expression. The primer sequences used are shown in Table S3.

### Immunostaining

Immunostaining analysis was performed as described previously with some modifications (Mae et al., 2018). For 2D cultures, the cells were fixed with 4% paraformaldehyde (PFA)/PBS for 20 min at 4°C. After washing with PBS twice, the cells were blocked with 1% normal donkey serum (MERCK) and 3% bovine serum albumin (BSA; Nacalai tesque)/PBT (PBS/0.25% Triton X-100, Nacalai tesque) for 1 h at room temperature. Primary antibodies were diluted with blocking solution at 1:500 and incubated with the samples overnight at 4°C. After washing with PBT twice, secondary antibodies diluted with blocking solution at 1:500 were incubated for 1 h at room temperature.

For the immunostaining analysis of frozen sections, samples were fixed with 4% PFA/PBS for 1 h at 4°C. Fixed samples were treated with 30% sucrose (Nacalai tesque)/PBS and frozen with OCT compound (Tissue-Tek) to make frozen sections by cryosectioning. The frozen sections were washed with distilled water and incubated with blocking solution for 1 h at room temperature. Primary antibodies except for PRKCζ were diluted with blocking solution at 1:500 and incubated with the samples overnight at room temperature. PRKCζ antibody was diluted at 1:50. After washing with distilled water twice, the sections were incubated with secondary antibodies diluted with blocking solution at 1:500 for 1 h at room temperature. Fluorescence images were captured by a BZ-X700 (KEYENCE). Image analysis was performed using a BZ-X Analyzer (KEYENCE).

For 3D imaging analysis, we applied Clear, Unobstructed Brain/Body Imaging Cocktails and Computational analysis (CUBIC) (Nojima et al., 2017; Susaki et al., 2015). After fixation with 4% PFA/PBS for 24 h at 4°C, the samples were treated with CUBIC1 solution diluted with distilled water at a 1:2 ratio on a seesaw shaker set at 30 rpm for 8 h at room temperature for tissue clearing. Then the samples were treated with CUBIC1 solution on the seesaw shaker at 30 rpm for 24 h at room temperature. After washing with PBS, the samples were incubated with blocking solution on the seesaw shaker at 30 rpm for 2 h at 4°C. Primary antibodies were diluted with blocking solution and incubated with the samples on the seesaw shaker at 30 rpm for 24 h at 4°C. After washing with blocking solution, the samples were incubated with secondary antibodies on the seesaw shaker at 30 rpm for 24 h at 4°C. After washing with PBS twice, the samples were treated with CUBIC2 solution diluted with PBS at a 1:2 ratio on the seesaw shaker at 30 rpm for 8 h at room temperature. Then the samples were treated with CUBIC2 solution on the seesaw shaker at 30 rpm for 24 h at room temperature and fluorescence images were captured by a Zeiss LSM710 (Zeiss). Details of the antibodies used in this study are shown in Key Resources Table. Image analysis was performed using ZEN 2 blue edition (Zeiss). CUBIC1 solution is a mixture of urea (10% final concentration, Nacalai tesque), Quadrol (25% final concentration, Tokyo Chemical Industry), Triton X-100 (5% final concentration), 5 M NaCl and distilled water. CUBIC2 solution is a mixture of urea (25% final concentration), sucrose (50% final concentration), triethanolamine (10% final concentration, Wako) and distilled water.

## QUANTIFICATION AND STATISTICAL ANALYSIS

### RNA sequencing data processing

FPKM values were calculated from mapped reads by normalizing to total counts and transcripts. Differentially expressed genes were detected using the DESeq2 package (version 1.20.0). The list of differentially expressed genes detected by DESeq2 (basemean > 5 and fold-change < 0.25, or basemean > 5 and fold-change > 4) were used for GO enrichment analysis by the clusterProfiler package (Yu et al., 2012).

### Single cell RNA sequencing data processing

The deconvolution of UMIs and cell barcodes of BCL files were conducted using bcl2fastq 2.20.0.422 and resulted in cell-specific FASTQ files (Illumina). Alignment to the human reference genome GRCh38 and UMI counting were conducted using the Cell Ranger v3.1.0 pipeline (10 × Genomics). Dimensionality reduction was carried out using the Uniform Manifold Approximation and Projection (UMAP) algorithm, and the cell clusters were visualized using Seurat package v3.1.1. Genes with adjusted *P*-values < 0.05 and fold-change ≥ 2.0 in the Tukey-Kramer test were considered as differentially expressed genes (DEGs) and used in the signal pathway analysis using Ingenuity Pathway Analysis software (QIAGEN). Heatmaps were generated using the pheatmap function of R package v3.6.1.

### Statistical analysis

Data of the flow cytometry and cell count analyses are presented as the mean ± SE, and the statistical analyses were performed on EZR (Kanda, 2013). Statistical analysis for the difference between two groups was performed using Student's t test. Differences were considered significant when $p < 0.05$.